ORIGINAL ARTICLE

# rGO-Cu@$TiO_2$ Nanocomposite: Photosynthesis, Characterization, and Dye Sensitized Solar Cell Performance

**Zaid H. Mahmoud[1*], Ghadir Kamil Ghadir[2], Hayder Musaad Al-Tmimi[3], Mustafa Jassim Al-Saray[4], Saeb Jasim Al-Shuwaili[5], Abdulkareem M. Mohammed[6], Ahmed Muzahem Al-Ani[7], Noor Alhuda Mohammad Ali Khalil[8], Mohammed Ahmed Mustafa[9]**

[1] *Chemistry Department, College of Science, University of Diyala, Iraq*

[2] *College of Pharmacy, Al-Farahidi University, Iraq*

[3] *College of Health Medical Techniques, Al-Bayan University, Iraq*

[4] *Department of Anesthesia Techniques, Al-Manara College For Medical Sciences, Maysan, Iraq*

[5] *Department of Anesthesia Techniques, Al-Hadi University College, Baghdad, 10011, Iraq*

[6] *Collage of Pharmacy, National University of Science and Technology, Dhi Qar, 64001, Iraq*

[7] *Department of Medical Engineering, Al-Nisour University College, Baghdad, Iraq*

[8] *College of Health and Medical Technology, Al-Ayen University, Thi-Qar, 64001, Iraq*

[9] *Department of Medical Laboratory Technology, University of Imam Jaafar AL-Sadiq, Iraq*

*Corresponding Author: Zaid H. Mahmoud
Email: zaidhameed_91@yahoo.com

Received: 23 February 2024 / Accepted: 22 March 2024



## Abstract

**Purpose:** In this work, nanocomposite with different weight ratios reduce graphene oxide/copper doping-anatase (rGO/Cu-$TiO_2$) has been successfully prepared using the photolysis method to evaluate the role of rGO/Cu in photovoltaic properties performance application as a photoanodes.

**Materials and Methods:** The X-Ray Diffraction (XRD), Raman spectrum, and X-Ray Photoelectron (XPS) results analysis confirmed successfully incorporating rGO/Cu in the $TiO_2$ crystal structure. Transmission Electron Microscopy (TEM) reveals the formation of spherical agglomeration nanoparticles with a size approximately equal to 18nm.

**Results:** The current density–voltage curves (J-V) and Intensity-Modulated Photocurrent Spectroscopy (IMPS) showed that the incorporation of rGO sheets enhances the ability of N3 loading of (rGO/Cu-$TiO_2$) photoanodes with faster charge transfer.

**Conclusion:** Our results illustrate that optimal Cu and rGO can increase the efficiency of dye-sensitized solar cells (4.56%) by 8.2% higher than $TiO_2$ DSSCs (3.52%).

**Keywords:** Dye Sensitized Solar Cells; X Ray Photoelectron; Photolysis; Intensity Modulated Photocurrent Spectroscopy; Selected Area Electron Diffraction.


DOI:

## 1. Introduction

The photoanode plays a major role in refining the performance of Dye-Sensitized Solar Cells (DSSCs) [1, 2]. The role of the photoanode cannot be ignored because it is accountable for the easy transfer mechanism of photoelectrons and supplying an active site for the adsorption of dye. So, it is significant to promote a photoanode with good surface area and excellent electric properties [3, 4]. Among different semiconductor oxides, Titanium Oxide ($TiO_2$) has been extensively studied and reported in the literature [5-7]. It has been observed that $TiO_2$ is sensitive to the choice of materials because of individual chemical and physical properties and a good corresponding level of electronic energy to the molecules of dye [8]. Despite its excellent properties, it has some limitations, but it still has some negative sides, such as a large band gap of ~3.2 eV and boosted recombination of charge carriers [9]. These factors obviously affect the utilization of solar radiation effectively solar radiation and then the conversion of power efficiency of DSSCs. However, last year, these problems enticed major concern in the literature and studies, and the authors and researchers have suggested different methods to treat these problems. This includes designing the $TiO_2$ electronic structure to restrict the recombination of charge carriers and then boosting its performance [10-12]. The electrical and optical features of $TiO_2$ can be significantly altered by introducing or incorporating other ion dopants in $TiO_2$ structure leading to alters in the levels of electronic energy via creating new bands or overlapping with $TiO_2$ electronic bands, and these alters can enhance its response in the visible region [13]. It is a known fact that the activity of $TiO_2$ can be improved clearly by incorporating transition ions, and carbon compounds such as CNTs, GO, and rGO [14, 15]. Between different carbon materials, reduced Graphene Oxide (rGO) is a reasonable material because of its excellent properties like eminent electric conductivity, high surface area, and relatively high optical transmittance [16]. Two years ago, Cao *et al.* [17] prepared semi-transparent photoanodes containing rGO/$TiO_2$ at room temperature and discovered that the efficiency conversion is 6.75%. On the other hand, Rusoma *et al.* synthesized photoanodes containing rGO/$TiO_2$ and showed a photo conversion energy of 7.15%. Lastly, the studies showed that co-incorporating elements have unrivaled advantages compared to single doping, which can improve and boost the performance of $TiO_2$ photocatalytic [18]. Previous studies have shown that doping $TiO_2$ with $Cu^{2+}$ can enhance; (1) enhanced optical response, (2) decrease bandgap, (3) improve the efficiency of power conversion, restrain recombination of charge carrier, and (5) increase loading of dye [19-21]. In addition, the incorporation of Cu into $TiO_2$ can accelerate the generation of photocharge carriers, leading to an increase in Jsc and then DSSCs PEC. Moreover, the last studies have illustrated that incorporating Cu in $TiO_2$ enhanced the Voc [22]. Venkatraman *et al.* developed an anatase/3% rGO nanocomposite for DSSCs and showed a PCE of 6.58% [23]. However, few papers and studies have investigated of incorporated Cu with rGO, considering the literature wealth in this field, but the studies and results were encouraging [24]. Therefore, it is highly desirable to explore active pathways for the synthesis of Cu/rGO@$TiO_2$ and investigate their real-world applications.

In this study, we reported the incorporated $TiO_2$ by Cu/rGO for efficient DSSCs. The active anode materials were prepared using photolysis and Hummer modified method, and then covered by the doctor blade process. We found that Cu@rGO doping $TiO_2$ has successfully enhanced the transport, photoactivity, and interfacial properties evident via the elaboration of the efficiency of DSSCs.



## 2. Materials and Methods

All chemical materials were supplied by Sigma Aldrich and Merck Company and utilized without any future purification.

### 2.1. Materials

Reagent grade copper nitrate hydrate ($Cu(NO_3)_2.4H_2O$), Titanium Chloride ($TiCl_4$), urea ($CH_4N_2O$) and Indium Tin Oxide (ITO) were supplied from Sigma Aldrich, while sodium nitrate ($NaNO_3$), sulfuric acid ($H_2SO_4$), graphite, Potassium Permanganate ($KMnO_4$), Hydrogen peroxide ($H_2O_2$) and cis-bis(isothiocyanato)bis(2,2-bipyridyl-4,4-dicarboxylato) ruthenium (II) dye were purchased from Merck company.

### 2.2. Synthesis of $Cu_2$+ Incorporate $TiO_2$

Pure and $Cu^{2+}$: $TiO_2$ nanocomposite was prepared by utilizing the photolysis method. For synthesis pure

anatase $TiO_2$, 0.2M of $TiCl_4$, and (5ml, 0.1M) urea as a surfactant agent were mixed and stirred for 30 min to get a homogenous solution. After that, the mixture was transferred to a manual irradiation system with 125W as shown in Figure 1. The full procedure of the manual irradiation system was listed by Zaid *et al.* [1]. The mixture was continuously irradiated until getting a white precipitate. Then, the precipitate was isolated and washed several times with acetone, ethanol, and deionized water. Finally, it dried at 75 °C for 3h and calcined for 5h at 550 °C. For the prepared Cu:$TiO_2$ nanocomposite, copper nitrate as a source of $Cu^{2+}$ was initially added to titanium chloride and urea at different (1, 5, and 10) wt.% weight ratios.

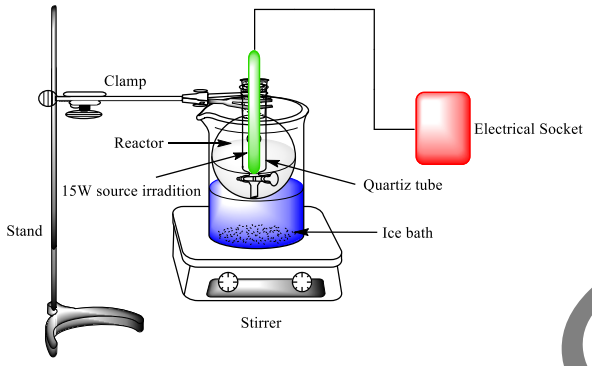


**Figure 1.** Manual irradiation system

## 2.3. Preparation of Cu-Doped $TiO_2$/rGO as Anode Electrodes

For synthesis of Cu incorporate $TiO_2$/rGO nanocomposite, a different amount (1, 5, and 10) wt.% Cu with $TiO_2$ was added to 5wt.% rGO. Briefly, GO solution was prepared using hammer modified method [25] and followed to reduce the product by hydrazine hydrate to get reduced graphene oxide (rGO) [26]. After that, it was dispersion in 10ml distilled water using an ultrasonic device and was then added to Cu-Ti solution with continuous stirring at 50 °C for 3h, followed by sonication for 1 h at room temperature. Then, the mixture was isolated, washed with acetone and distilled water several times, and dried for 4h at 70 °C.

## 2.4. Assemble of DSSCs

The substrate of indium tin oxide glass (ITO, 83% trans, and 8 ohm) was cut in a 3*3 dimension and dipped conductive side in $TiCl_4$ to make a blocking layer. By using scotch tape, the active area was defined and equal to 2*2 $cm^2$. The slurry bastes of pure and wt.% rGO/$Cu^{2+}$ incorporated $TiO_2$ were prepared by mixing an appropriate amount of PEG as a binder, ethanol, and distilled water with powder of synthesized materials, then it was coated on the conductive slide of ITO by using drop casting. After that, the substrate was calcined at 450 °C for 2h to remove PEG. After cooling, the substrates were dipped in an $N_3$ dye solution for 24h, and then washed using absolute ethanol to eliminate the anchored dye molecules. The thickness of casting pure and wt.% rGO/$Cu^{2+}$ incorporated $TiO_2$ was determined using a profilometer SJ-210 and it was found about 20 µm. The counter electrodes were fabricated by precipitating CNTs on the conductive side of another piece of ITO. Finally, the anode and cathode were connected by sandwiching between 0.1 iodine electrolyte solution. The curves of photocurrent-voltage (I-V) were recorded under irradiation halogen lamp with a power of 100 mW/$cm^2$. The principal work of prepared solar cells is shown in Figure 2a, b. The DSSCs parameters were calculated from the following equation [27] (Equation 1):

$$FF = \frac{I_{max} \times V_{max}}{V_{oc} \times I_{sc}} \quad (1)$$

Where FF: represents to fill factor, $I_{max}$, and $V_{max}$ mention the maximum value of current and voltage, while $V_{oc}$ and $I_{sc}$ back to open-circuit voltage and short-circuit current. The efficiency of conversion energy is calculated as follows (Equation 2):

$$n = \frac{V_{oc} \times I_{sc} \times FF}{P_{in}} \quad (2)$$

# 3. Results and Discussion

## 3.1. Characterization of Synthesized Nanocomposite

The XRD pattern of pure and rGO/Cu incorporated $TiO_2$ is shown in Figure 3(a-d). In Figure 3a, The diffraction peaks at 2θ 25.46°, 38.01°, 48.19°, 54.32°, 63.07° and 69.13° are corresponding to (101), (104), (200), (105) and (211), which in agreement with formation of the pure tetragonal anatase phase of $TiO_2$

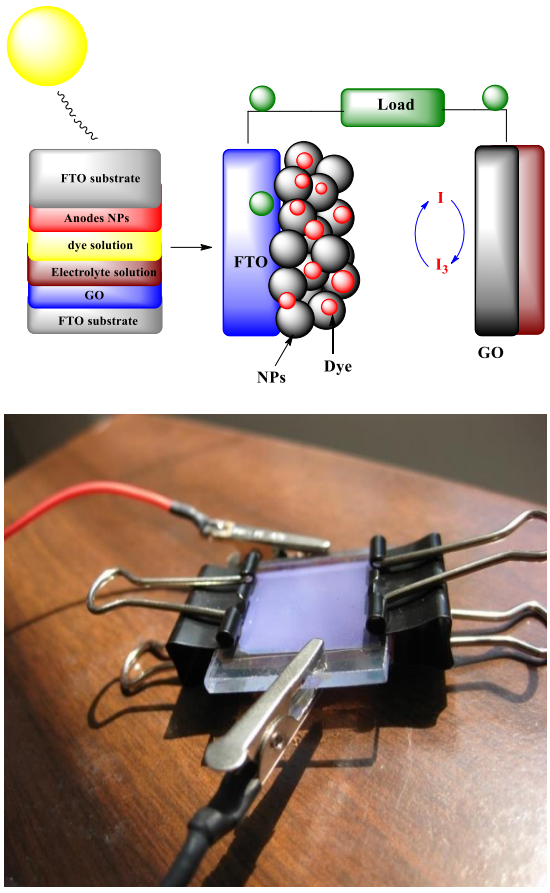


**Figure 2.** (a) schematic diagram of DSSCs working, (b) fabricate DSSC

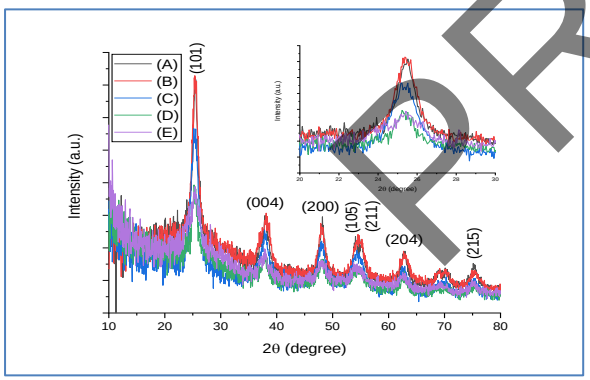


**Figure 3.** XRD of (a) $TiO_2$, (b-d) 1,5 and 10wt.% rGO/Cu-$TiO_2$

(JCPDS 21-1272) [28]. After incorporating rGO (Figure 3b-d), as can be understood from the XRD results, all diffraction peaks correspond with a decrease in intensity compared to pure $TiO_2$, as well as, there were no peaks assigned to Cu and rGO in the synthesized composite, which may be attributed to the lower concentration of rGO and Cu, as noted via other researchers [29]. Another reason could be the overlapping of the diffraction peak of $TiO_2$ (101) with a characteristic peak of rGO at 24.65o. All XRD results indicated no phase transformation in the $TiO_2$ structure.

The crystallite size of pure and rGO/Cu incorporated $TiO_2$ was investigated by using the Scherre Equation 3 [30]:

$$D = \frac{0.9}{\beta cos\theta} \quad (3)$$

The results are summarized in Table 1. The results show that increasing the content of rGO/Cu leads to a decrease in crystallite size, which may be attributed to the segregation of dopants on the $TiO_2$ bonders, causing particles to become hindered [31]. On the other hand, the incorporation of high-radius ions of rGO/Cu inside the $TiO_2$ crystal lattice leads to an increase in the d-spacing and the result pushes the peaks to lower positions. Moreover, most literature work on the analysis of XRD results is focused on demonstrating the crystallite size by utilizing the FWHM and the Scherrer equation and neglecting strain contributions and lattice distortions. To address this issue, the Williamson-Hall equation is used [32]. As shown in Figure 4, the plot includes βcosθ versus 4sinθ and is defined as the Williamson-Hall plot which aims to plot a line with a slope corresponding to the microstrain value. On the other hand, the y-intercept corresponds to the crystallite size and is obtained using the following Equation 4:

$$\beta cos\theta = K\lambda/D + 4\varepsilon sin\theta \quad (4)$$

Where $\varepsilon$ represents the residual strain. From the plot, the y-intercept represents to crystallite size mean as well as, the Williamson-Hall plot shows that the values of slop are very small, which mentions that the structure of prepared materials includes microstrain with a small amount. The results shown (Table 1) are differences between the crystallite size obtained from the Williamson-Hall plot and Scherre equation, which can be attributed to the presence of strain.

For more chemical structural investigation, Raman spectroscopy is considered an efficient instrument for it. The Raman spectrum of pure GO, rGO, and wt.% Cu/GO incorporated $TiO_2$ are shown in Figure 5a-d. The results show many recognized bands. For $TiO_2$, four main peaks centered at 175, 415, 530, and 655 $cm^{-1}$ corresponding to Eg1, $B_1g$, $A_1g+B_1g$, and Eg2 active modes, respectively. On the other hand, the

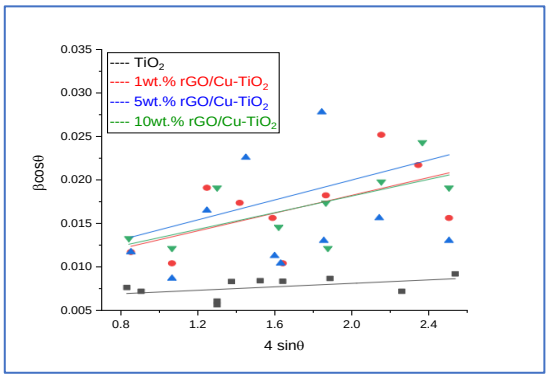


**Figure 4.** Williamson-Hall plot of pure and wt.% rGO/Cu-$TiO_2$

spectrum shows two eminent peaks located at 1375 and 1610 $cm^{-1}$, which are assigned to the D and G bands of rGO dopant. Moreover, the results showed increasing the ID/IG ratio with increasing rGO/Cu dopant content, which indicates the production of more $sp^3$ carbon in synthesized compound. In addition, the characterized peak of rGO at 1375 shifted to a lower wavenumber after the reaction with $TiO_2$, which may be back to the stress produced by agglomeration $TiO_2$ and growth on the surface of rGO sheets, and this confirms the incorporation of rGO [33].

The chemical state and chemical composition of rGO/Cu-$TiO_2$ were investigated by XPS analysis and the results are shown in Figure 6a-e. Figure 6a displays the survey spectrum of rGO/Cu-$TiO_2$ and rGO, in which the element C, O, Ti, and Cu are shown clearly. Figure 6(b-d) shows the O 1s, C 1s, and Cu 2p spectrum, respectively. As displayed in Figure 6b, the XPS spectra of O 1s for rGO are different after incorporation with $TiO_2$ in the position and shape of peaks. In the rGO state, the spectra at 531.8 eV are assigned to a hydroxyl group, while the spectrum at 530.1 eV is attributed to Ti-O-C in rGO/Cu-$TiO_2$, which indicates the strong interaction between rGO and $TiO_2$ [33]. The spectra C 1s of rGO and of rGO/Cu-$TiO_2$ are shown in Figure 6c, which shows that the C 1s intensity of rGO is much higher than in rGO/Cu-$TiO_2$. In the state of rGO, three peaks located at 284, 286.5, and 283.1eV correspond to C-C, C=C, and C-O. As clearly appeared in the XPS spectra, the strength of the oxygenic functional group is reduced in rGO/Cu-$TiO_2$, proposing that some of the oxygenic groups are decreased after incorporation with $TiO_2$. In Figure 6d, two peaks are centered at 933.1 and 952.5 eV binding energy corresponding to Cu $2p_{1/2}$ and $2p_{3/2}$, respectively, which indicate successfully incorporating Cu in $TiO_2$ crystal structure [34].

The morphology of prepared materials was investigated using TEM. The TEM images with corresponding selected area electron diffraction patterns (SAED) of pure and rGO/Cu incorporated $TiO_2$ are shown in Figure 7a-d. The image appeared to spherical shapes particles with uniform morphology, as well as, it well distributed on the surface of rGO sheets. An identical morphology pattern was noted via images in his work. On the other hand, the size of particles for all prepared materials was predestine in the range of 10-35nm. Moreover, the results showed that the 1wt.% rGO/Cu-$TiO_2$ has lower particle size than pure $TiO_2$, which indicates that the addition of rGO/Cu hinders the particle growth of $TiO_2$ and hence, enhances the surface area of prepared materials and thereby increases the ability of dye loading. Moreover, the SEAD pattern of 5%rGO/Cu-$TiO_2$ appears as shining concentric rings product via diffraction from planes of (101), (004), (200), and (105) for $TiO_2$, showing the polycrystalline nature.

The spectrum properties of pure and wt.% rGO/Cu-$TiO_2$ were investigated using a UV-Vis spectrophotometer in the range of 250-500nm. Figure 8a shows the adsorption spectra of prepared materials, which depicts the adsorption edge of pure $TiO_2$ that is located at approximately 390nm.



**Table 1.** Parameters and particle size of pure and wt.%rGO/Cu-$TiO_2$

| **photoanodes** | 2θ of (101) crystal plane | Lattice parameter (°A) | FWHM | D (Scherre) (nm) | $D_{W-H}$ (nm) | Strain |
|---|---|---|---|---|---|---|
| **$TiO_2$** | 25.46° | a=b=3.78 c=9.5023 | 0.6703 | 13 | 25 | 0.0054 |
| **1wt.%rGO/Cu-$TiO_2$** | 25.40° | a=b=3.78 c=9.5123 | 0.9464 | 9 | 18 | 0.0062 |
| **5wt.%rGO/Cu-$TiO_2$** | 25.32° | a=b=3.78 c=9.5167 | 0.9852 | 8 | 17 | 0.0070 |
| **10wt.%rGO/Cu-$TiO_2$** | 25.24° | a=b=3.78 c=9.5205 | 0.9931 | 7 | 16 | 0.0059 |

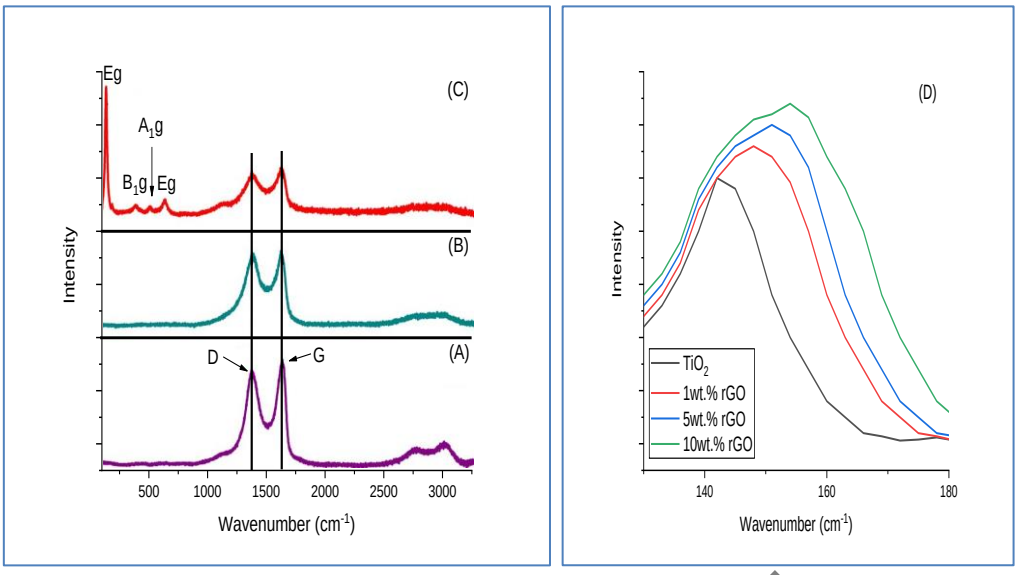


**Figure 5.** Raman spectrum of (a) GO, (b) rGO, (c) 5wt.% rGO/Cu-TiO2, and (d) Eg peak intensity of $TiO_2$

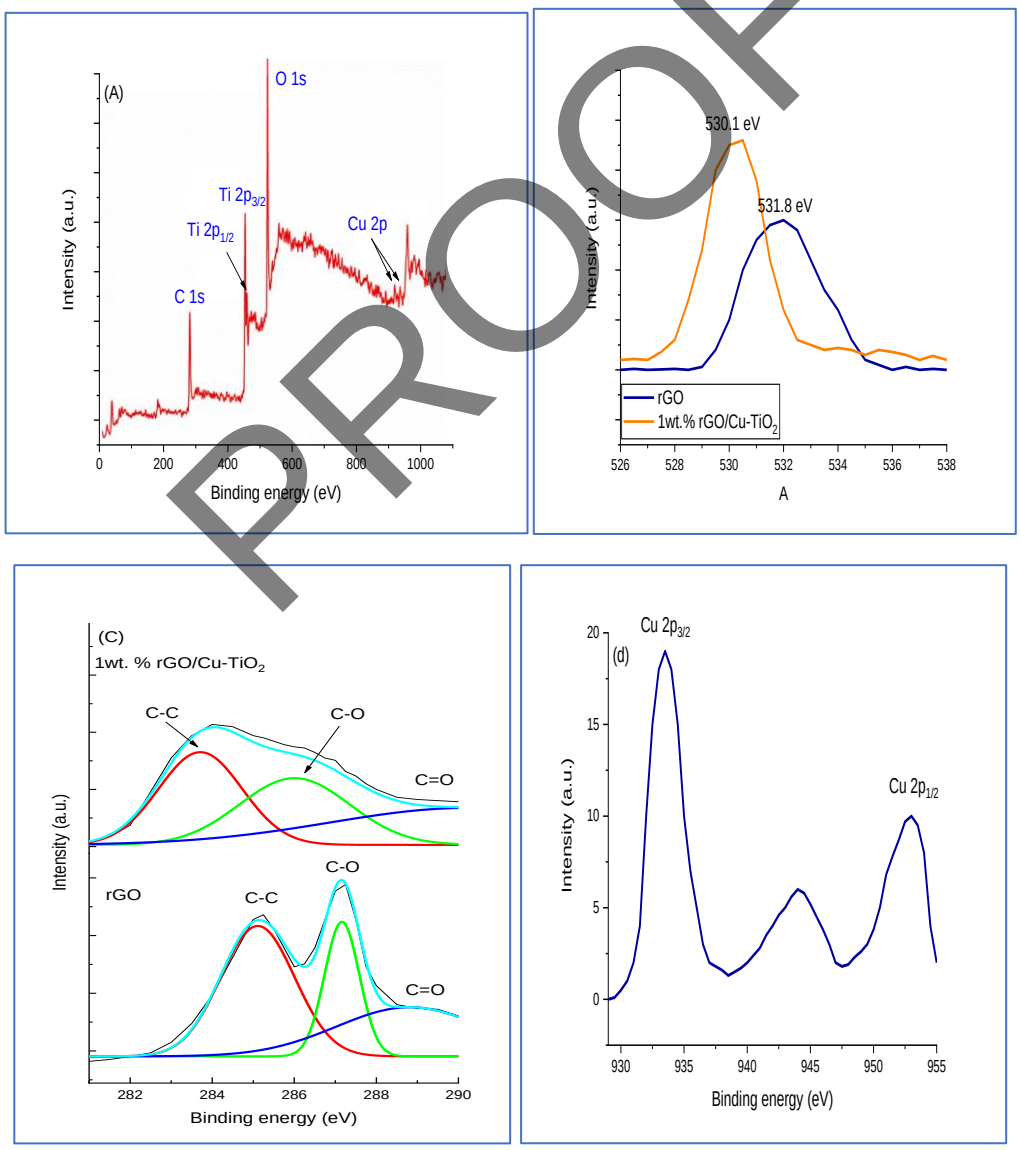


**Figure 6.** XPS of (a) survey spectrum, (b) O 1s peak, (c) C 1s peaks, and (d) Cu 2p peaks

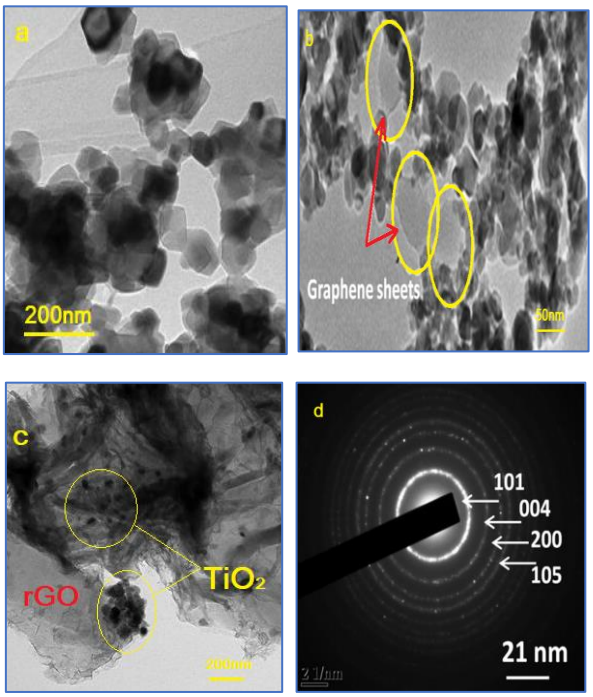


**Figure 7.** TEM of (a) pure $TiO_2$, 1wt.% rGO/Cu-$TiO_2$, (c) 10wt.% rGO/Cu-$TiO_2$, and (d) SAED of pattern

However, the incorporation of rGO and Cu with $TiO_2$ shifted the edge toward a high wavelength to the visible region. The edge shifting can be back to either the p-2p orbital hybridization between rGO and $TiO_2$ or to the formation of new electronic levels below the conduction band of $TiO_2$ assign to Cu ions incorporating [35]. This contribution enables the electron of $TiO_2$ to transfer to conduction band easily, and hence, inhibition of the recombination process and enhances the efficiency of charge transport [36]. By using the Kubelka-Munk function [37], the band gap was calculated for the prepared nanocomposite and it equals 2.95, 2.40, 1.74 and 1.69 eV for the $TiO_2$ and 1, 5, and 10% rGO/Cu-$TiO_2$, respectively. According to band gap results (Figure 8b), The bandgap of pure $TiO_2$ was reduced with increasing rGO/Cu content, because of a boost in the minimum energy demanded for transferring electrons from VB to CB. To determine the dye adsorption amount on the surface of photoanodes, UV-Vis spectroscopy was used to investigate the $N_3$ dye desorbed with 0.2mM NaOH, and the results are illustrated in Table 1 and Figure 8c. As can be shown, the introduction of rGO/Cu increases the adsorption ability of $N_3$ dye, which contributes to increasing Jsc and PCE [38]. The results clearly show that 5wt.% rGO/Cu dopant-based photoanode has a discrete advantage over another photoanode in dye adsorption. On the other hand, the increasing rGO/Cu content has a negative effect on the cohesion of $N_3$ dye and the area of photoadsorption because of boosted aggregation, causing decreased Jsc and low PCE of the DSSC.

The PL analysis was used to study and investigate the recombination electron-hole state in synthesized nanocomposite and the results are shown in Figure 9. The intensity of PL was decreased with increasing the rGO/Cu till 5wt.% dopant, appearing delay in recombination rate because of effective charges transport as the content ratio boosted, hence, increasing the electron injection at photoanode/$N_3$ dye [39].

To estimate the impact of rGO incorporating on the porosity and surface area of Cu/$TiO_2$, $N_2$ adsorption-desorption performance was carried out. The BET method was used for the calculation of specific surface area and the results are shown in Figure 10. The results appear that, according to IUPAC isotherm classification, bare $TiO_2$ showed a type II, which was distinctive to a nonporous compound with lower adsorption of nitrogen gas because of its smaller surface area (12.55 $m^2/g$). Obviously, a high surface area was obtained by incorporating samples, where results show largest surface area of 120.74 $m^2/g$ for Cu/$TiO_2$ nanocomposite with IV isotherm type that indicates a mesoporous compound. rGO/Cu-$TiO_2$ demonstrated the BET surface area with type IV isotherm and H1 hysteresis loop at P/Po = 0.8-0.9 according to large mesopore characteristics. Moreover, the results illustrated reducing in surface area with rGO incorporating because of the high particle agglomeration. On the other hand, the results revealed that the rGO incorporating Cu/$TiO_2$ was significantly effective for boosting a specific surface area of the solar cell performance, which boosted about 9-10 times compared with bare $TiO_2$. These properties cause a more efficient contact surface between the photocatalyst and the dye and more speed in electrons transferring

### 3.2. DSSC Performance Analysis

To evaluate the effect of rGO/Cu dopant on the performance of photovoltaic for fabricated photoanodes, four discrete dye sanitized solar cell-based anatase and different wt.% rGO/Cu was invented. Figure 11a shows the response of the J-V

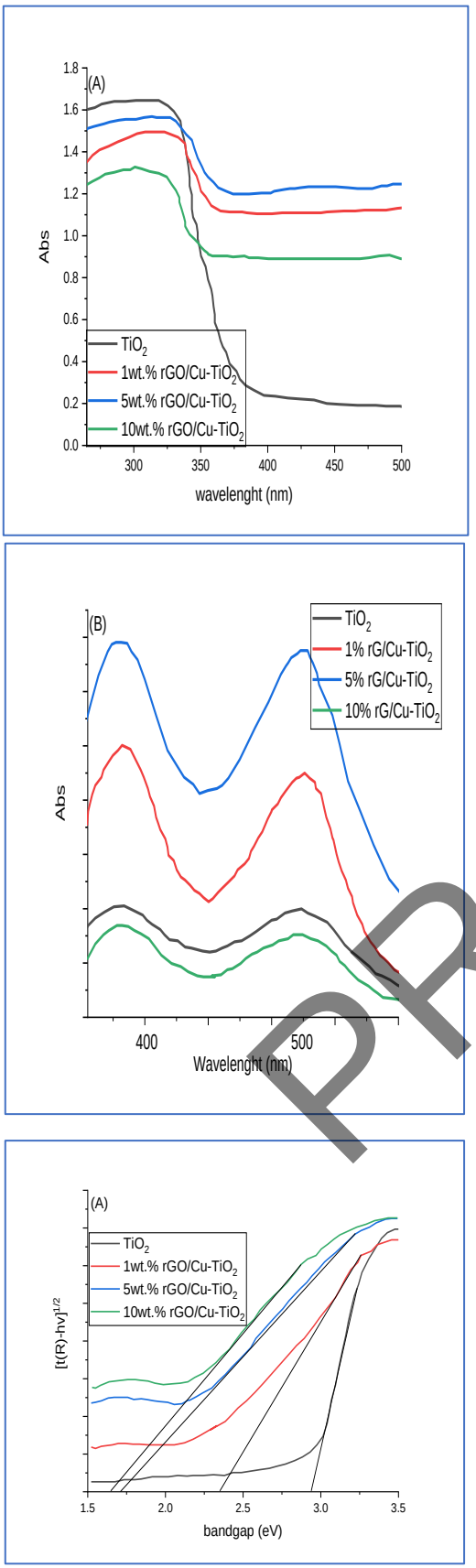


**Figure 8.** (a) UV-Vis spectrum of pure and wt.%rGO/Cu-$TiO_2$, (b) band gap, and (c) UV-Vis spectrum of dye adsorption on pure and wt.%rGO/Cu-$TiO_2$

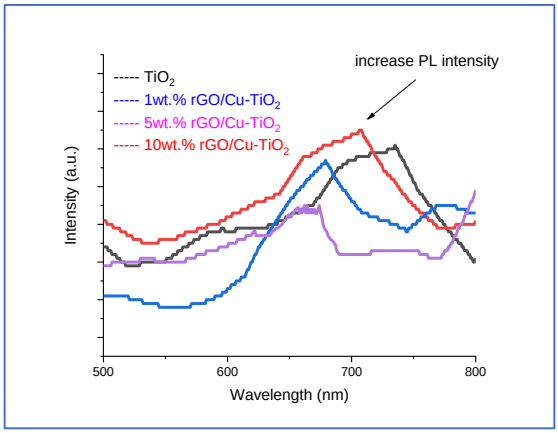


**Figure 9.** PL spectrum of pure and wt.% rGO/Cu-$TiO_2$ nanocomposite

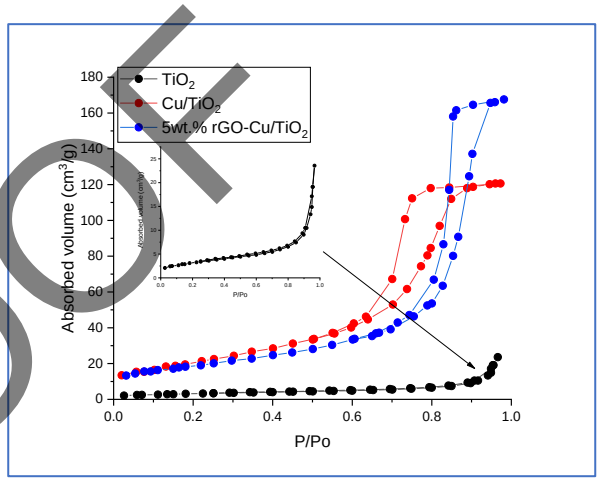


**Figure 10.** BET of bare, Cu, and 5wt.%r GO/Cu-$TiO_2$

curve from different fabricated DSSCs, and the values of Voc, Jsc, FF, and η are summarized in Table 2. The results show that the pure $TiO_2$ DSSCs showed a PCE of 3.52% with Jsc and Voc of 14.74mA and 0.482V, respectively, while the photovoltaic properties were enhanced with incorporating rGO/Cu and it showed an efficiency of 4.62%. The Cu-incorporating can have a dual impact on the fabricated solar cells. The first impact is to enhance the Voc by 9.6% approximately, compared with pure $TiO_2$ DSSC, proposing that incorporating Cu decreases the band gap [40]. The second impact is that the arrival of Cu led to structural defects, which do as the site of recombination and reduce Jsc of fabricated DSSCs [41]. Moreover, the doping of rGO sheets easies the ability of dye loading, charge separation, and electron mobility prevents recombination of charge carriers, and then increases Jsc [42]. These results illustrated that the synergetic

impact of rGO and Cu can ease the separation of charge carriers, and adsorption of dye and then enhances Jsc and Voc [43]. However, this negative impact was noted in 10wt.% rGO/Cu incorporation based $TiO_2$ DSSC. The IPCE spectra of different fabricated rGO/Cu-$TiO_2$ DSSCs photoanodes are demonstrated in Figure 11b. The incorporating $TiO_2$ by rGO assists in increasing the specific surface area, as well as, enhances the ability of dye loading, hence more electrons were injected from excited $N_3$ dye to CB of $TiO_2$. While, incorporating Cu assists in increasing Voc and then leading to improved PCE of fabricated DSSCs. The incorporation of $TiO_2$ by rGO/Cu illustrates a high efficiency of conversion with a large response of photocurrent edge. The results show (Figure 11b) the same trend of Jsc values as obtained in Figure 11a. In addition, the IPCE of wt.%rGO/Cu-$TiO_2$ based DSSCs enhanced highly, mention that the $N_3$ dye about the synthesized nanocomposite can reaper more photons in the visible region. This boost is more considerable at 570nm approximately that corresponding wt.%rGO/Cu-$TiO_2$ nanocomposite adsorption peak. From IPCE spectra, the results showed a conversion efficiency of 85%, noted from 5wt.% rGO/Cu-$TiO_2$ compared with pure $TiO_2$. On the other hand, a 10wt.% dopant illustrated a low value of IPCE because of the agglomeration of dye on the surface, increased recombination state of charges, and hence poor transport of charges, and these results are in agreement with the literature [44]. For more DSSCs investigation, the IMPS was carried out for evaluating the time of electron transport of fabricated DSSCs. All measurements were performed at 0.5-2.5 V and are summarized and presented in Figure 11c. The results showed that all measurements of 5wt.% rGO/Cu-$TiO_2$ DSSCs showed considerably lower time of transfer compared with other fabricated DSSCs, as well as, the average time of electron transport for pure and 1, 5, and 10wt.% rGO/Cu-$TiO_2$ based $TiO_2$ were 2.5, 1.8, 1.3, and 3.4ms, respectively, which indicates enhanced mobility of electrons because of reduced bandgap and excellent transfer of electrons through graphene sheets [45]. The IMPS results are in agreement with IPCE and J-V values.

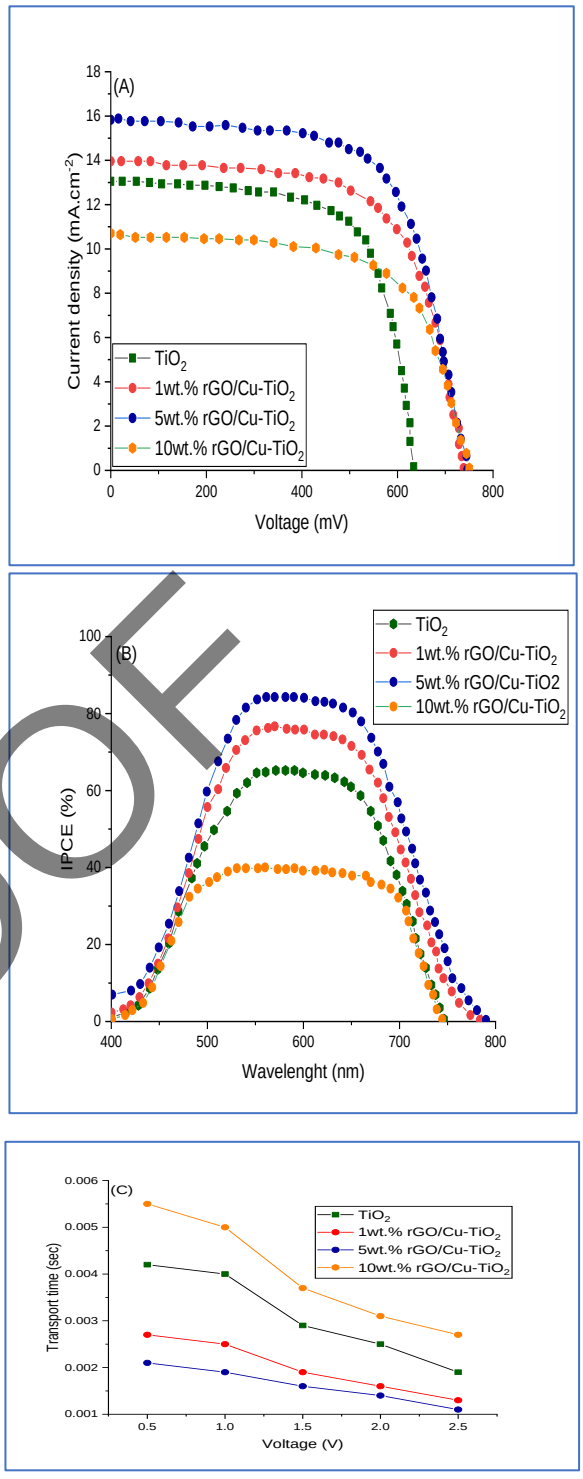


**Figure 11.** (a) J-V curves of prepared photoanodes, (b) IPCE of prepared photoanodes, (c) IMPS measurements of transport time

**Table 2.** DSSCs parameters with different pure and wt.% rGO/Cu-$TiO_2$ photoanode

| Fabricated DSSCs | Jsc | Voc | FF | η |
|---|---|---|---|---|
| **$TiO_2$** | 11.75 | 461.83 | 0.65 | 3.52 |
| **1%rGO/Cu-$TiO_2$** | 12.97 | 476.42 | 0.59 | 3.64 |
| **5%rGO/Cu-$TiO_2$** | 14.74 | 482.56 | 0.60 | 4.26 |
| **10%rGO/Cu-$TiO_2$** | 9.30 | 552.66 | 0.64 | 3.28 |

## 4. Conclusion

Briefly, our results have appeared that an appropriate incorporation of rGO and Cu in anatase considerably enhances the efficiency of DSSCs. Incorporating or rGO considerably enhanced the ability of $N_3$ dye loading, hence increasing the current density (Jsc) and efficiency of fabricated solar cells. Moreover, suitable Cu doing improves the open circuit voltage (Voc), thereby assisting in getting higher efficiency. Moreover, the average rate of electron transfer for 5wt.% rGO/Cu-$TiO_2$ nanocomposite was achieved to be 45% less than pure $TiO_2$ nanoparticles. The results show that doping 5wt.% Cu and 5wt.% rGO, the DSSCs product a 4.26%, which more 9.5% relative to pure $TiO_2$ based DSSCs. Hence, the results of our study support a rapid method and are economically applicable to forming active DSSCs.

## References


1- Mahmoud, Z.H., AL-Bayati, R.A. & Khadom, A.A. Electron transport in dye-sanitized solar cell with tin-doped titanium dioxide as photoanode materials. *J Mater Sci: Mater Electron 33*, 5009–5023 (2022). https://doi.org/10.1007/s10854-021-07690-9

2- ZH Mahmoud, RA Al-Bayati, AA Khadom, Enhanced photovoltaic performance of dye-sanitized solar cell with tin doped titanium dioxide as photoanode materials, *Chalcogenide Letters*, *18*(12), (2021).

3- Wang, C., Zhu, Y., Ge, Z., *et al.*, 2020. The feasible photoanode of graphene oxide/zinc aluminum mixed metal oxides for the dye-sensitized solar cell. *Colloid Interf. Sci. Commun. 39* (100), 313.

4- Xu, Z., Li, Y., Li, Y., Yuan, S., Hao, L., Gao, S., Lu, X., 2020. Theoretical study of T shaped phenothiazine/carbazole based organic dyes with naphthalimide as π-spacer for DSSCs. Spectrochim. *Acta Mol. Biomol. Spectrosc. 233*, 118201. https://doi.org/10.1016/j.saa.2020.118201.

5- Zaid H Mahmoud, Reem Adham AL-Bayati, Anees A Khadom, The efficacy of samarium loaded titanium dioxide (Sm: TiO2) for enhanced photocatalytic removal of rhodamine B dye in natural sunlight exposure, *Journal of Molecular Structure*, *1235*, 2022. https://doi.org/10.1016/j.molstruc.2021.132267

6- Mahmoud, Z.H., AL-Bayati, R.A. & Khadom, A.A. Synthesis and supercapacitor performance of polyaniline-titanium dioxide-samarium oxide (PANI/TiO2-Sm2O3) nanocomposite. *Chem. Pap. 76*, 1401–1412 (2022). https://doi.org/10.1007/s11696-021-01948-6

7- Mohammed Alwan Farhan, Zaid Hamid Mahmoud, Marwa Sabbar Falih, Synthesis and characterization of TiO2/Au nanocomposite using UV-Irradiation method and its photocatalytic activity to degradation of methylene blue, *Asian J. Chem.*, *30*(5), 1142-1146, 2018.

8- Noor Sabah Al-Obaidi, Zainab Esmail Sadeq, Zaid H Mahmoud, Ahmed Najem Abd, Anfal Salam Al-Mahdawi, Farah K Ali, Synthesis of chitosan-TiO2 nanocomposite for efficient Cr (VI) removal from contaminated wastewater sorption kinetics, thermodynamics and mechanism, *Journal of Oleo Sciences*, *72*(3), 337-346.

9- Mohammed Asaad Mahdi, Mohammed A Farhan, Zaid H Mahmoud, Ahmed Mahdi Rheima, Zainab sabri Abbas, Mustafa M Kadhim, Asala Salam Jaber, Safa K Hachim, Ahmad Hussain Ismail, Direct sunlight photodegradation of congo red in aqueous solution by TiO2/rGO binary system: Experimental and DFT study, *Arabian Journal of Chemistry*, *16*(8) 104992. https://doi.org/10.1016/j.arabjc.2023.104992

10- González-Verjan, V.A., Trujillo-Navarrete, B., Félix-Navarro, R.M. *et al.* Effect of TiO2 particle and pore size on DSSC efficiency. *Mater Renew Sustain Energy 9*, 13 (2020). https://doi.org/10.1007/s40243-020-00173-7

11- Kaur, N., Singh, D.P. & Mahajan, A. Plasmonic Engineering of TiO2 Photoanodes for Dye-Sensitized Solar Cells: A Review. *J. Electron. Mater. 51*, 4188–4206 (2022). https://doi.org/10.1007/s11664-022-09707-3

12- Putri, A.A., Kato, S., Kishi, N. *et al.* TiO2/Bi5O7I Composite Films for Dye-Sensitized Solar Cells. *J. Electron. Mater. 49*, 1827–1834 (2020). https://doi.org/10.1007/s11664-019-07868-2

13- Li, Z., Yu, L. Double-layered TiO2 cavity/nanoparticle photoelectrodes for efficient dye-sensitized solar cells. *Front. Mater. Sci. 17*, 230638 (2023). https://doi.org/10.1007/s11706-023-0638-8

14- Liu, L., Zhang, Y., Zhang, B. *et al.* A detailed investigation on the performance of dye-sensitized solar cells based on reduced graphene oxide-doped TiO2 photoanode. *J Mater Sci 52*, 8070–8083 (2017). https://doi.org/10.1007/s10853-017-1014-9

15- Lee, CH., Kim, K.H., Bark, C.W. *et al.* Preparation of doping metal TiO2 particle/nanotube composite layer and their applications in dye-sensitized solar cells. *Met. Mater. Int. 19*, 1355–1359 (2013). https://doi.org/10.1007/s12540-013-0640-2

16- Tang, B., He, Y., Zhang, Z. *et al.* Influence of N doping and the functional groups of graphene on a RGO/TiO2 composite photocatalyst. *Sci. China Technol. Sci. 63*, 1045–1054 (2020). https://doi.org/10.1007/s11431-019-9749-1

17- Gao, N., Wan, T., Xu, Z., Ma, L., Ramakrishna, S., Liu, Y., 2020. Nitrogen doped TiO2/Graphene nanofibers as DSSCs photoanode. *Mat. Chem. Phy. 255*, 123542. https://doi.org/10.1016/j.matchemphys.2020.123542.

18- Pattarith, K., Areerob, Y. Fabrication of Ag nanoparticles adhered on RGO based on both electrodes in dye-sensitized

solar cells (DSSCs). *Renewables 7*, 1 (2020). https://doi.org/10.1186/s40807-020-00058-3

19- Dhonde, M., Sahu, K., Murty, V.V.S., Nemala, S.S., Bhargava, P., Mallick, S., 2018. Enhanced photovoltaic performance of a dye sensitized solar cell with Cu/N Co doped TiO2 nanoparticles. *J Mater Sci Mater Electron. 29* (8), 6274.

20- Gupta, A., Sahu, K., Dhonde, M., Murty, V.V.S., 2020. Novel synergistic combination of Cu/S co-doped $TiO_2$ nanoparticles incorporated as photoanode in dye sensitized solar cell. *Solar Energy. 203*, 296–303.

21- Dhonde, M., Sahu, K., Murty, V.V.S., 2021. Microwave-assisted hydrothermal synthesis of Cu-doped TiO2 nanoparticles for efficient dye-sensitized solar cell with improved open-circuit voltage. *Inter. Jour Ener. Reser. 45*, 5423–5432.

22- Raghvendra S. Dubey*, Sandesh R. Jadkar, and Ajinkya B. Bhorde, Synthesis and Characterization of Various Doped TiO2 Nanocrystals for Dye-Sensitized Solar Cells, *ACS Omega 2021*, 6, 5, 3470–3482. https://doi.org/10.1021/acsomega.0c01614.

23- Ramakrishnan V, N. M, Pitchaiya S, S. A, Pugazhendhi A, Velauthapillai D. UV-aided graphene oxide reduction by $TiO_2$ towards $TiO_2$/reduced graphene oxide composites for dye-sensitized solar cells. *Int J Energy Res. 2020*;1–13. https://doi.org/10.1002/er.5806.

24- Pham, *et al.*, 2015. Cu-doped TiO2/reduced graphene oxide thin-film photocatalysts: Effect of Cu content upon methylene blue removal in water. *Ceram. Intern. 41*, 11184–11193.

25- Regkouzas, P., Sygellou, L. & Diamadopoulos, E. Production and characterization of graphene oxide-engineered biochars and application for organic micro-pollutant adsorption from aqueous solutions. *Environ Sci Pollut Res 30*, 87810–87829 (2023). https://doi.org/10.1007/s11356-023-28549-y

26- Abdolhosseinzadeh, S., Asgharzadeh, H. & Seop Kim, H. Fast and fully-scalable synthesis of reduced graphene oxide. *Sci Rep 5*, 10160 (2015). https://doi.org/10.1038/srep10160

27- Atia, D.M., Ahmed, N.M. Mathematical modeling, parameter identification, and electrical performance of a DSSC based on nature-inspired optimization techniques. *J Comput Electron 22*, 723–741 (2023). https://doi.org/10.1007/s10825-023-02018-8

28- Kužel, R., Nichtová, L., Matěj, Z. *et al.* X-ray Diffraction Investigations of TiO2 Thin Films and Their Thermal Stability. *MRS Online Proceedings Library 1352, 1031* (2011). https://doi.org/10.1557/opl.2011.1133

29- Wang, N., Zhang, F., Mei, Q. *et al.* Photocatalytic TiO2/rGO/CuO Composite for Wastewater Treatment of Cr(VI) Under Visible Light. *Water Air Soil Pollut 231, 223* (2020). https://doi.org/10.1007/s11270-020-04609-8

30- Zitting, A., Paajanen, A. & Penttilä, P.A. Impact of hemicelluloses and crystal size on X-ray scattering from atomistic models of cellulose microfibrils. *Cellulose 30*, 8107–8126 (2023). https://doi.org/10.1007/s10570-023-05357-8

31- Tetiana A. Dontsova, Anastasiya S. Kutuzova, Kateryna O. Bila, Svitlana O. Kyrii, Iryna V. Kosogina, Daria O. Nechy poruk, Enhanced photocatalytic activity of TiO2/SnO2 binary nanocomposites. *J.Nanomater. (2020).* https://doi.org/10.1155/2020/8349480

32- F.K. Mammo, I.D. Amoah, K.M. Gani, L. Pillay, S.K. Ratha, F. Bux, S. Kumari, Microplastics in the environment: inter actions with microbes and chemical contaminants. *Sci. Total Environ.* (2020). https://doi.org/10.1016/j.scitotenv.2020.140518

33- Sha, J. *et al.* In situ synthesis of ultrathin 2-D TiO2 with high energy facets on graphene oxide for enhancing photocatalytic activity. *Carbon 68*, 352–359 (2014).

34- Jia, Z., Wang, F., Xin & Zhang, B. Simple Solvothermal routes to synthesize 3D BiOBrxI1-x microspheres and their visible-light-induced photocatalytic properties. *Ind. Eng. Chem. Res. 50*, 6688–6694 (2011).

35- Irfan, F., Tanveer, M.U., Moiz, M.A. *et al.* TiO2 as an effective photocatalyst mechanisms, applications, and dopants: a review. *Eur. Phys. J. B 95, 184* (2022). https://doi.org/10.1140/epjb/s10051-022-00440-8

36- Çorlu, T., Tekin, S., Karaduman Er, I. *et al.* Room-temperature gas sensing properties of Zn, Sn and Cu-doped TiO2 films. *J Mater Sci: Mater Electron 34, 2224 (2023).* https://doi.org/10.1007/s10854-023-11609-x

37- Rescigno, R., Sacco, O., Venditto, V. *et al.* Photocatalytic activity of P-doped TiO2 photocatalyst. *Photochem Photobiol Sci 22*, 1223–1231 (2023). https://doi.org/10.1007/s43630-023-00363-y

38- Dhonde, M., Sahu, K., Murty, V.V.S., Nemala, S.S., Bhargava, P., Mallick, S., 2018. Enhanced photovoltaic performance of a dye sensitized solar cell with Cu/N Co doped TiO2 nanoparticles. *J Mater Sci Mater Electron. 29* (8), 6274.

39- Tehmina Akhtar, Habib Nasir, Effat Sitara, Syeda Aqsa Batool Bukhari, Sharif Ullah, Rana Muhammad Arslan Iqbal, Efficient photocatalytic degradation of nitrobenzene by copper-doped TiO2: kinetic study, degradation pathway, and mechanism, *Environ Sci Pollut Res Int. 2022* Jul;29(33):49925-49936. doi: 10.1007/s11356-022-19422-5.

40- Aleksandra Bartkowiak, Oleksandr Korolevych, Gian Luca Chiarello, Malgorzata Makowska-Janusik, Maciej Zalas, Experimental and theoretical insight into DSSCs mechanism influenced by different doping metal ions, *Applied Surface Science, vol. 597*, 153607, 2022. https://doi.org/10.1016/j.apsusc.2022.153607

41- S. Meng, E. Kaxiras, Electron and Hole Dynamics in Dye-Sensitized Solar Cells: Influencing Factors and Systematic Trends, *Nano Lett., 10* (2010), pp. 1238-1247.

42- A. Kubiak, Z. Bielan, A. Bartkowiak, E. Gabała, A. Piasecki, M. Zalas, A. Zielińska-Jurek, M. Janczarek, K. Siwińska-Ciesielczyk, T. Jesionowski, Synthesis of Titanium Dioxide via Surfactant-Assisted Microwave Method for Photocatalytic and Dye-Sensitized Solar Cells Applications, *Catalysts.*, *10* (2020), p. 586.

43- L.B. Patle, V.R. Huse, A.L. Chaudhari, Band edge movement and structural modifications in transition metal doped TiO2 nanocrystals for the application of DSSC, *Mater. Res. Express.*, *4* (2017)

44- D. Pysch, A. Mette, S.W. Glunz, A review and comparison of different methods to determine the series resistance of solar cells Sol. *Energy Mater. Sol. Cells.*, *91* (18) (2007), pp. 1698-1706.

45- Y. Wang, R. Zhang, J. Li, L. Li, S. Lin, First-principles study on transition metal-doped anatase TiO2, *Nanoscale Res. Lett.*, *9* (2014), p. 46.